Available online at www.sciencedirect.com

ScienceDirect

journal homepage: www.elsevier.com/locate/he

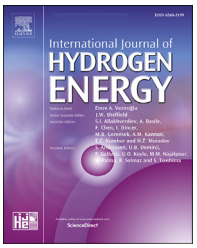

Numerical study of an industrial burner to optimise NO_x emissions and to evaluate the feasibility of hydrogen-enriched fuel

Senthilathiban Swaminathan [a,b,*], *Christoph Spijker* [a], *Zlatko Raonic* [a], *Michael Koller* [c], *Irmela Kofler* [b], *Harald Raupenstrauch* [a]

[a] *Chair of Thermal Processing Technology, Montanuniversität Leoben, Franz Josef-Straße 18, 8700 Leoben, Austria*
[b] *Area 3, Low Carbon Energy Systems, K1-MET GmbH, Stahlstraße 14, 4020 Linz, Austria*
[c] *Ebner Industrieofenbau GmbH, Ebner-Platz 1, 4060 Leonding, Austria*

HIGHLIGHTS

- Implementation of a two-step numerical model to analyse an Industrial Burner.
- Validation with Sandia Flame D experiments and Industrial burners.
- Computational optimisation techniques to reduce the computation time.
- Modification of primary to secondary air mass flow ratio to reduce NO_x emissions by a factor of 0.845.
- 76.8% reduction in CO and 41.8% increase in NO when enriching Natural Gas with 50% of Hydrogen.

ARTICLE INFO

Article history:
Received 17 April 2023
Received in revised form
12 July 2023
Accepted 28 July 2023
Available online xxx

Keywords:
NO_x
Flamelet model
Primary air ratio
Hydrogen enrichment
Detailed chemistry

ABSTRACT

Reducing NO_x emissions from industrial burners is a significant concern due to their harmful environmental and human health impact. A computationally efficient numerical model was developed and validated using a detailed GRI 3.0 chemistry mechanism to simulate the combustion process and precisely predict the NO_x emissions from industrial burners. The numerical model was implemented to reduce NO_x emissions by varying the burner's primary to secondary air mass flow ratio. An optimum nozzle diameter was proposed to abate NO_x emissions by a factor of 0.845. A feasibility study on the optimised burner was conducted by blending up to 50% hydrogen by volume with natural gas by maintaining the same burner power output. Results showed that the burner exhibited similar flame characteristics until 40% hydrogen was added to natural gas. A 41.8% increase in NO and a 76.8% decrease in CO emissions were observed by enriching natural gas with 50% hydrogen.

* *Corresponding author*. Area 3, Low Carbon Energy Systems, K1-MET GmbH, Stahlstraße 14, 4020 Linz, Austria.
E-mail address: senthilathiban.swaminathan@k1-met.com (S. Swaminathan).

https://doi.org/10.1016/j.ijhydene.2023.07.328

1. Introduction

NO_x emissions, mainly nitric oxide and nitrogen dioxide, can cause photochemical smog, acid rain, reduction in ozone concentrations and various health impacts [1]. According to the EEA [2] report, in 2020, the manufacturing and extractive industry contributed 15% of NO_x emissions, and 14% of NO_x emissions emerged from the energy supply sector. Furthermore, 64,000 premature deaths in Europe could be traced to overexposure to NO_2 concentrations. The Austrian Government has committed to reducing 69% of the nitrogen oxide emissions by 2030 against the measured emission values from 2005 [3].

These NO_x emissions can be reduced by pre-combustion, combustion modification and post-combustion techniques. Pre-combustion techniques mainly involve treating the fuel or replacing air with pure oxygen, which is expensive. Combustion modification techniques comprise reducing the amount of oxygen or the flame temperature as the NO_x formation depends on flame temperature, stoichiometric ratio and mixing degree of air and fuel. These can be achieved through technologies such as Low Excess Air, Burners Out of Service, Over Fire Air, Air Staged Low NO_x Burner, Fuel Staged Low NO_x Burner and Flue Gas Re-circulation. Post-combustion techniques consist of treating the emissions from the exhaust gas by chemical, physical or biological processes. These post-combustion methods help in reducing NO_x to a greater extent. The most common post-combustion technique used is selective catalytic reduction [4].

Extensive research experiments and mathematical models have been developed to understand the behaviour of NO_x emissions from industrial burners. One of them is the flamelet model, which is widely used by researchers to study turbulent combustion. Lopez-Ruiz et al. [5] developed a numerical model for hydrogen diffusion flames to reduce NO_x emissions by flame splitting method and investigated the model with different flame power outputs. To precisely predict the NO_x emissions, Pitsch [6] modified the unsteady flamelet model with a Eulerian approach by considering the local fluctuations of the scalar dissipation rate. Vreman et al. [7] investigated premixed and non-premixed flamelets with large-eddy simulations. They concluded that the transport equation must be solved for the NO mass fraction with sub-grid chemistry models to predict the emissions of nitric oxides. Vujanović et al. [8] developed a post-processor for predicting NO_x emissions with a reduced chemistry mechanism using thermal and prompt NO. It could be recognised from these literature studies that the flamelet model is unable to predict NO_x emissions correctly, so either a modification in the flamelet model or a post-processing step is required. This is because of the lower order of the chemical reactions time scale by the nitrogen oxide formation path during the combustion, which results in improper predictions of NO_x emissions from the flamelet model. Hence, a post-processor was developed by Pollhammer et al. [9] with a detailed chemistry model. The available numerical model by Pollhammer et al. [9] is optimised further for reducing the computational effort by Swaminathan et al. [10].

With the recent developments, more and more countries are introducing new regulations for industries to reduce carbon dioxide emissions. The latest research has shown that using hydrogen or blending hydrogen in the fuel mixture shows a promising reduction in carbon dioxide emissions. Nonetheless, it is also essential to observe that using hydrogen as a fuel will increase nitrogen oxide emissions [11,12]. Zhang et al. [13] conducted an experimental study to investigate the effect of diluent gas with different hydrogen fractions and analysed the flame propagation characteristics on a premixed flame. Van Der Drift et al. [14] did an experimental study on ceramic foam burners and detected that increasing the hydrogen concentration in the fuel mixture by more than 70% can cause flashback in burners designed for low NO_x emissions with premixed natural gas and air. Therefore, it is necessary to investigate whether the burner considered for modelling in this study is able to use larger hydrogen concentrations in the fuel mixture. Choudhuri and Gollahalli [15] found that increasing the hydrogen concentration in the fuel mixture on diffusion flames reduces CO emissions and increases NO_x emissions. Cozzi and Coghe [16] conducted experiments on a non-premixed swirled flame and discovered that both CO and NO_x emissions increase until 80% of hydrogen is added to the fuel mixture. Accordingly, it is required to analyse the effect of hydrogen enrichment in natural gas on emissions for the desired effect, i.e. maintaining the power output of the burner constant. In this study, the optimised numerical model [9,10] is utilised to predict the NO_x emissions from an industrial burner and then enhanced by modifying the burner's primary to secondary air ratio to reduce the NO_x emissions. The improved burner design is then investigated with different hydrogen-enriched natural gas compositions containing 0%, 10%, 20%, 30%, 40% and 50% of hydrogen by volume. The flame characteristics of different fuel mixtures and their CO, CO_2, NO and NO_2 emissions are presented in detail.

2. Numerical model

The developed model uses a two-step approach to predict NO_x emissions. Firstly, the flamelet approach was used to solve for velocity, pressure and temperature considering radiation contribution. The basic continuity and momentum equations were solved along with $k-\varepsilon$ turbulence model using the libOpenSmoke library developed by Cuoci et al. [17,18] in OpenFOAM [19]. The obtained solution is then transferred to the NO_x model [9,10] and solved with a detailed reaction mechanism. The following sections explain the flamelet model, NO_x model, model validation with experiments and optimisation techniques to improve the computational efficiency of the NO_x model.

The turbulent flow is solved using Reynolds-Averaged Navier-Stokes (RANS) model with the following partial differential equation system defining the conservation of mass, impulse and enthalpy, respectively:

$$\begin{aligned}
&\frac{\partial \rho}{\partial t}+\nabla\cdot(\rho\overline{u})=0\\
&\frac{\partial \rho\overline{u}}{\partial t}+\nabla\cdot(\rho\overline{u}\overline{u})=\nabla p+\nabla\cdot\overline{\tau}-\nabla\cdot(\rho \mathrm{R})+f_b\\
&\frac{\partial \rho\widetilde{H}}{\partial t}+\nabla\cdot(\rho\overline{u}\widetilde{H})=\nabla\cdot(\alpha_t\nabla\widetilde{H})+\mathrm{Q}_r
\end{aligned} \tag{1}$$

Please cite this article as: Swaminathan S et al., Numerical study of an industrial burner to optimise NO_x emissions and to evaluate the feasibility of hydrogen-enriched fuel, International Journal of Hydrogen Energy, https://doi.org/10.1016/j.ijhydene.2023.07.328

where u denotes the velocity vector, p is the pressure, R is the Reynolds stress tensor, τ denotes velocity induced stress tensor, H is the enthalpy, Q_r is the radiation source term, α_t is the thermal diffusivity, and f_b stands for the gravitational force. The turbulent transport properties, turbulent viscosity and conductivity of the fluid are calculated using $k-\varepsilon$ turbulence model [20]. Radiative heat transfer in the system with relatively high combustion temperature and participating medium has a significant influence on the total heat transfer in the system. The last term, Q_r, in the enthalpy equation, is evaluated using a radiative heat transfer equation in the s direction within the discrete ordinates method (DOM) [21]:

$$\frac{I_\lambda}{ds} = \hat{s}\cdot\nabla I_\lambda = \kappa_\lambda I_{b\lambda} - \beta_\lambda I_\lambda + \frac{\sigma_{s\lambda}}{4\pi}\int_{4\pi} I_\lambda(\hat{s}_i)\Phi_\lambda(\hat{s}_i,\hat{s})d\Omega_i \quad (2)$$

where I_λ is the radiation intensity, $I_{b\lambda}$ is the radiation intensity of spectral black body, κ_λ is the absorption coefficient, $\sigma_{s\lambda}$ stands for the scattering coefficient, $\beta_\lambda = \kappa_\lambda + \sigma_{s\lambda}$ is the extinction coefficient, and Φ_λ is the scattering phase function. Radiation propagation is solved without scattering, whereas the composition-dependent absorption coefficient is modelled using weighted-sum-of-gray-gases model [22].

2.1. Flamelet model

Numerical modelling of non-premixed combustion is based on the steady laminar flamelet model, assuming that the local flame structure consists of a large number of laminar flamelets. Under the assumption of much smaller chemistry time scales compared to turbulent mixing, i.e. for very large Damkoehler numbers, chemistry adapts instantaneously to the flow conditions. Furthermore, combustion takes place in a very thin reaction zone, which is sufficiently small and doesn't interact with the turbulent length scales. Counterflow flame configuration enables one-dimensional formulation for the flamelet transport equations under given conditions, in the direction normal to the stoichiometric surface with the scalars as a function of mixture fraction [23]:

$$\rho\frac{\partial Y_i}{\partial t} = \frac{1}{2}\rho\chi\frac{\partial^2 Y_i}{\partial Z^2} + \dot{m}_i \quad (3)$$

$$\rho\frac{\partial T}{\partial t} = \frac{1}{2}\rho\chi\frac{\partial^2 T}{\partial Z^2} + \frac{\chi}{2c_p}\frac{\partial T}{\partial Z}\frac{\partial c_p}{\partial Z} + \sum_{i=1}^{n}\rho\frac{\chi}{2}\frac{c_{p_i}}{c_p}\frac{\partial Y_i}{\partial Z}\frac{\partial T}{\partial Z} - \sum_{i=1}^{n}\frac{h_i}{c_{p_i}}\dot{m}_i \quad (4)$$

where ρ is the density, Y_i stands for the mass fraction of the chemical species, Z is the mixture fraction, T is the temperature, c_p and c_{p_i} are the mixture and species specific heat at constant pressure respectively, h_i stands for the specific enthalpy of species and $\dot{m}_i$ is the reaction rate.

In order to consider the non-adiabatic combustion state, laminar flamelets for different stoichiometric scalar dissipation rates χ_{st} are calculated for different enthalpy defects ϕ_H, where enthalpy defect is defined as the difference between actual enthalpy H and the adiabatic enthalpy value. Using libOpenSmoke [17,18] utilities, laminar flamelet profiles are calculated for each enthalpy defect considering temperature and mass fraction changes with the methodology described above. The flamelet profiles were created with 200 points for a range of scalar dissipation rates starting from 1×10^{-5} Hz and continued until the flame was extinguished. And these flamelet profiles are generated for positive enthalpy defects ranging from 0 to 500 kJ/kg and for negative enthalpy defects ranging from −5 kJ/kg and continued until the flame extinguishes. An in-house equilibrium flamelet generator was also used to create flamelet profiles for higher negative enthalpy defects when the libOpenSmoke tool was unable to create the desired flamelet profiles.

Subsequently, generated laminar flamelet profiles are extended to describe the turbulent flame front implementing a statistical method, i.e. probability density functions (PDF). The mean value $\widetilde{\phi}$ of every physical quantity $\phi(Z, \chi_{st}, \phi_H)$ is approximated by the joint probability density function as the product of the statistically independent distributions for each parameter: mixture fraction Z, scalar dissipation rate χ_{st} and enthalpy defect ϕ_H. With the tabulated chemistry, only two additional Favre-averaged transport equations, one for mixture fraction Z and another for mixture fraction variance Z'', are solved within the RANS context [23].

$$\frac{\partial\overline{\rho}\widetilde{Z}}{\partial t} + \nabla\cdot(\overline{\rho u}\widetilde{Z}) = \nabla\cdot\left(\frac{\mu_t}{Sc_t}\nabla\widetilde{Z}\right)$$
$$\frac{\partial\overline{\rho}\widetilde{Z''^2}}{\partial t} + \nabla\cdot(\overline{\rho u}\widetilde{Z''^2}) = \nabla\cdot\left(\frac{\mu_t}{Sc_t}\nabla\widetilde{Z''^2}\right) + \frac{2\mu_t}{Sc_t}(\nabla\widetilde{Z})^2 - \overline{\rho}\widetilde{\chi}, \quad (5)$$

where Sc_t is the turbulent Schmidt number. After convergence has been reached for the steady-state case, all relevant flow fields are defined as the initial conditions for the transient modelling of the NO_x formation.

2.2. NO_x model

As mentioned in Section 1 and by other researchers [24,25], the flamelet model overestimates the NO_x emissions. Therefore a detailed chemistry model was implemented by Pollhammer et al. [9] as a successive modelling step. The converged flow parameters from the flamelet model are implemented as initial values for the NO_x model, and all species involved in the formation of the NO_x mechanism are reset to zero. The developed NO_x model solves only the transient species transport equation with the GRI 3.0 mechanism [26] in specific regions of the numerical domain. The regions are determined based on the relative change in the species mass fraction in every computational cell and the flame temperature.

$$\frac{\partial(\rho Y_i)}{\partial t} + \nabla\cdot(\rho u Y_i) - \nabla\cdot\mu_{eff}(\nabla Y_i) = RR(Y_i) \quad (6)$$

where Y_i is the species concentration, μ_{eff} is the effective turbulent viscosity, and $RR(Y_i)$ is the source term which is the reaction rate calculated from the detailed chemistry model. The above equation is solved in specific regions when the change in the species mass fraction is greater than 2.5% for all 53 species of the GRI 3.0 mechanism, and the whole numerical domain is updated every 200 iterations. Finally, the NO_x emissions were calculated by integrating the reaction rates of

Please cite this article as: Swaminathan S et al., Numerical study of an industrial burner to optimise NO_x emissions and to evaluate the feasibility of hydrogen-enriched fuel, International Journal of Hydrogen Energy, https://doi.org/10.1016/j.ijhydene.2023.07.328

nitric oxide and nitrogen dioxide over the entire domain after the simulation is converged.

2.3. Model validation

The numerical model was developed in OpenFOAM 2.4 and validated by Pollhammer et al. [9] in the Chair of Thermal Processing Technology with experimental data from Barlow and Frank [27] and also measured data from an industrial furnace. The experiment is used by various researchers [28–31] to validate numerical models, since the experiments are more reliable and have only 1% uncertainity in the temperature measurements [32]. The Sandia flame D experiment by Barlow and Frank [27] was conducted with a burner having a jet inner diameter (d) of 7.2 mm and a pilot outer diameter of 18.2 mm. The jet is composed of a mixture of 25% methane and 75% air at 293 K with a velocity of 49.6 m/s. The pilot inflow contains a lean mixture with a mixture fraction of 0.27 at 1880 K with a velocity of 11.4 m/s. The co-flow injects air at 295 K with a velocity of 0.9 m/s. The burner was modelled using a 2D axisymmetric approach, with a geometry of size 0.9 m in length and 0.3 m in radius. The flamelet tables were generated with libOpenSmoke [17,18] utility.

The simulation was performed with the flamelet model and compared with experimental data, as illustrated in Fig. 1a, along the axis of the burner nozzle. The temperature profile along the axis is in good accordance with the experimental data. The data from the flamelet model was used to initialise the NO_x Model, and the results from the NO_x model are compared with experimental data, as in Fig. 1b. The NO_x model underestimated the mass fraction of NO compared to the experimental data throughout the axis of the burner nozzle. On the other hand, these predictions are acceptable compared to extremely high values predicted from the flamelet model [24,25].

The model was also validated with an industrial furnace by Pollhammer et al. [9]. The model predicted 63 ppm of NO_x emissions compared to the measurement data of 65 ppm with ambient air temperature. In the case of preheated air with 472 K, the model predicted 78 ppm against the measurement value of 92 ppm. For further details about the validation of the industrial furnace, the reader is referred to Pollhammer et al. [9].

2.4. Optimisation of NO_x model

The developed numerical model was optimised further to reduce the computation time without affecting the accuracy of the predictions. Three different methods were investigated and analysed. The NO_x model solves only the species transport equation while the temperature field remains constant throughout the simulation. In OpenFOAM, during every iteration, the forward and reverse reaction rate constants are calculated based on the changing temperature field. In the developed NO_x model, it is unnecessary to calculate the reaction constants for every iteration. As a first step, to minimise the computational effort, the reaction rate constants are only calculated and stored in the first iteration, and those values are used in subsequent iterations. This method was able to produce the results faster with smaller mesh sizes, but when the number of computational cells was increased, the memory storage occupied by the reaction constants was very high and reduced the efficiency of the solver.

The second method to reduce the computation time was to initialise the computational domain with nitric oxide predictions from the Zeldovich mechanism [33,34] instead of initialising with zero species concentration. This method was able to reduce 31.8% of the computation time, and the accuracy of the NO_x predictions from this method can be seen in Fig. 1b. The third method to reduce the computation time was to use a mesh refinement only in the flame region and using a coarse mesh in other parts of the domain, as the solver computes only where the change in species concentration is more than 2.5%. With this method, an optimal mesh size was used by reducing the computational cells in regions devoid of flames, thereby resulting in a 36.5% reduction in computation time. These optimisation strategies are explained in detail at Swaminathan et al. [10] and Spijker et al. [35] and are not repeated here.

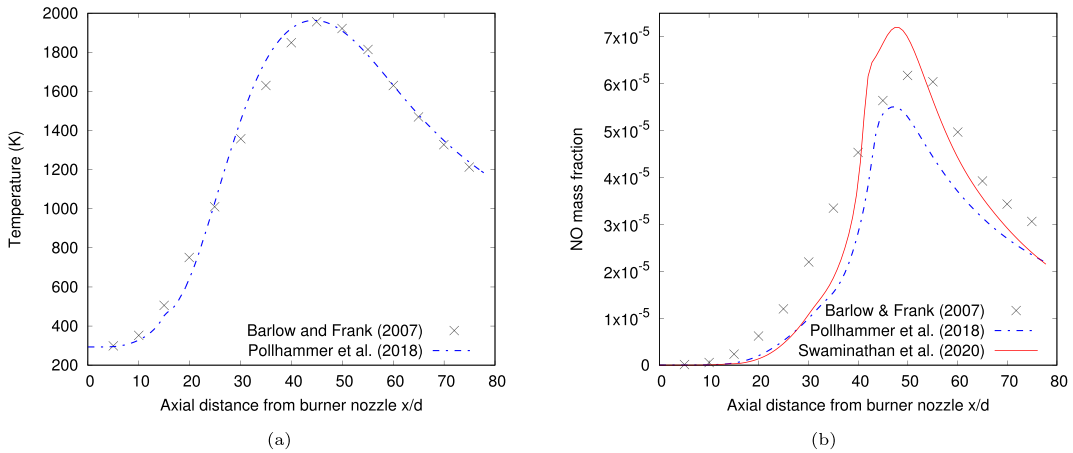

Fig. 1 – Model validation.

Please cite this article as: Swaminathan S et al., Numerical study of an industrial burner to optimise NO_x emissions and to evaluate the feasibility of hydrogen-enriched fuel, International Journal of Hydrogen Energy, https://doi.org/10.1016/j.ijhydene.2023.07.328

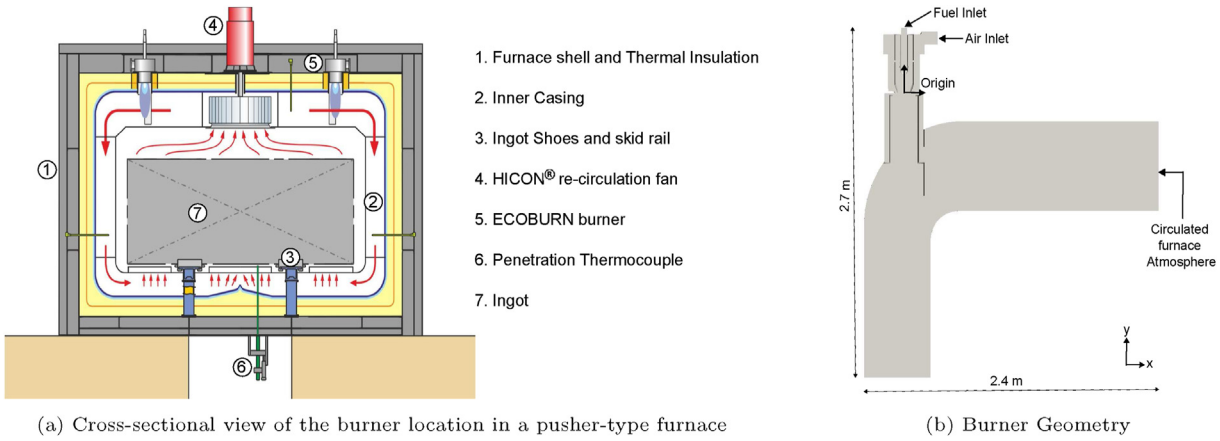

(a) Cross-sectional view of the burner location in a pusher-type furnace (b) Burner Geometry

Fig. 2 – Location of burner and burner geometry used for modelling.

3. Industrial burner

3.1. *Industrial burner properties*

The industrial burner considered for modelling is used in a pusher-type furnace used for the heat treatment of aluminium ingots before hot rolling. The aluminium ingots are heated with high convection via a nozzle field. Large circulation fans distribute the furnace atmosphere to the individual nozzles. To heat the recirculated furnace atmosphere, the gas burners are installed directly in the flow channels, as in section 2a. The burner is modelled with Solidworks software with the dimensions of 2.4 m long, 1.2 m wide and 2.7 m in height. The geometry consists of fuel inlet, air inlet and circulated furnace atmosphere, as shown in Fig. 2b. A mesh independence study was conducted with three different polyhedral meshes generated using ANSYS ICEM and Fluent meshing tools [36,37] with a refinement near the flame region, as mentioned in Table 1. The meshes were refined near the wall region to maintain y + values of less than 4. The temperature and mass fraction of CO_2 were measured at the outlet, and the change between medium and fine meshes was 0.13% for temperature and 0.017% for the mass fraction of CO_2. Hence, the investigations were conducted with burner mesh consisting of 6.2 million computational cells.

The burner is fuelled by natural gas at 300 K and uses air at 300 K as an oxidizer. The circulated furnace atmosphere is maintained at 723 K. The species composition of fuel, air and the circulated furnace atmosphere are mentioned in Table 2. The fuel and air inlet were initialised with the mixture fraction of 1 and 0, respectively. The exhaust air inlet was initialised with the enthalpy and mixture fraction values determined from the flamelet profile calculations. The standard wall functions available in OpenFOAM were applied for k and ε for the walls. The inlets were initialised with mass flow values as in Table 4, and the outlet was set up with constant atmospheric pressure.

Table 1 – Comparison of different meshes with temperature and mass fraction of CO_2 computed at the outlet.

Mesh	Number of Cells (in million)	Temperature (K)	CO_2 mass fraction (–)
Coarse	4.03	784.2	0.11535
Medium	6.2	777.23	0.11297
Fine	7.79	778.28	0.11299

Table 2 – Species Composition (in mole fractions).

Specie	Natural Gas	Air	Circulated Furnace Atmosphere
CH_4	0.9797	–	–
C_2H_6	0.0105	–	–
N_2	0.0087	0.79	0.733
CO_2	0.0011	–	0.072
O_2	–	0.21	0.051
H_2O	–	–	0.144

3.2. *Modelling for reducing NO_x emissions*

The mass flow of primary to secondary air ratio (m_p/m_s) for the burner was calculated from the converged flamelet model and was estimated to be 0.52. To further reduce the NO_x emissions, two different mass flow ratios of 0.4 and 1.4 were investigated by modifying the geometry of the burner. The

Table 3 – Species composition of different fuel mixtures (in mole fractions).

Specie	0% H_2	10% H_2	20% H_2	30% H_2	40% H_2	50% H_2
CH_4	0.9797	0.88173	0.78376	0.68579	0.58782	0.48985
C_2H_6	0.0105	0.00945	0.0084	0.00735	0.0063	0.00525
H_2	0	0.1	0.2	0.3	0.4	0.5
CO_2	0.0011	0.00099	0.00088	0.00077	0.00066	0.00055
N_2	0.0087	0.00783	0.00696	0.00609	0.00522	0.00435

Please cite this article as: Swaminathan S et al., Numerical study of an industrial burner to optimise NO_x emissions and to evaluate the feasibility of hydrogen-enriched fuel, International Journal of Hydrogen Energy, https://doi.org/10.1016/j.ijhydene.2023.07.328

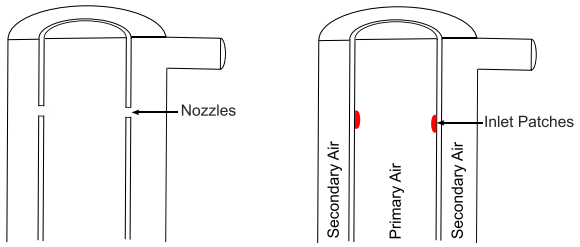

Fig. 3 – Simulation strategy used for modelling different mass flow ratios.

total airflow to the burner remains unchanged for all cases, and only the ratio of primary to secondary air was modified. To efficiently achieve the desired mass flow ratio, the nozzles connecting the primary and secondary tubes were removed from the burner and inlet patches were created in the location of nozzles as in Fig. 3. Replacing the nozzles with inlet patches made it simpler to set different mass flow ratios within the same burner geometry and was used only as a simulation strategy to reduce the computational effort. For both mass flow ratios of 0.4 and 1.4, the mass flow of primary air was equally divided between the number of nozzles and set as a mass flow boundary condition in the nozzle inlet patches. The mass flow of secondary air was set as a boundary condition in the air inlet patch. An optimum mass flow ratio for reducing the NO_x emissions was determined by simulating both the flamelet and the NO_x model for all three cases.

3.3. *Modelling for blending of hydrogen with natural gas*

The optimised burner geometry with reduced NO_x emissions was further investigated by mixing hydrogen with natural gas to estimate the influence of hydrogen blending on emissions. Five different fuel compositions containing 10%–50% of hydrogen by volume were studied, as mentioned in Table 3, and the carbon and nitrogen emissions were compared with natural gas (0% hydrogen). The lower heating value of different fuel mixtures was calculated from the lower heating value of methane (35.883 MJ/m^3) and hydrogen (10.783 MJ/m^3). The mass flow of the fuel mixture and the air was adjusted to maintain the same power output, and the mass flow of the circulated furnace atmosphere was maintained constant for all simulations. From Table 4, it can be observed that increasing the percentage of hydrogen reduces the mass flow of the fuel mixture and air to produce the same power output due to the lower heating value of the fuel mixture. For all fuel mixtures, the flamelet profiles are created as mentioned in Section 2.1, with both fuel and air temperature at 300 K. The temperature of the circulated furnace atmosphere is maintained at 723 K. Other boundary conditions are maintained the same as mentioned in Section 3.1.

4. Results and discussion

4.1. *Optimisation of NO_x emissions*

Skreiberg et al. [38] investigated the influence of temperature and air excess ratio on NO_x emissions. They observed that increasing the air excess ratio also increases the NO_x emissions and concluded that an increase in temperature alone could not influence the NO_x emissions. A further study was conducted by Houshfar et al. [39], stating that peak reduction in NO_x emissions could be obtained when the primary air excess ratio is maintained between 0.8 and 0.95. Spliethoff et al. [40] stated that temperature has a significance on NO_x emissions depending on the flue gas atmosphere, i.e. when the exhaust gas is air-rich, NO_x emissions are high. Accordingly, it is vital to investigate the excess air present in the combustion zone.

Initial investigations on oxygen mass fraction from the converged flamelet simulations indicate that the secondary air entering the combustion zone was still unburnt. It can be observed from Fig. 4e that unburnt oxygen is still left, surrounding the flame region, which results in the NO formation zones. Hence reducing the secondary air would also reduce the NO formation zones. Therefore, the mass flow ratio of $m_p/m_s = 1.4$ was implemented and investigated as the first optimisation technique. However, introducing excess air in the primary air resulted in higher velocities along the axis of the burner, even up to 160 m/s, as in Fig. 5a. These higher velocities modify the flame structure by widening the flame and making the flame longer. Consequently, the excess oxygen present around the flame region, as in Fig. 4f for $m_p/m_s = 1.4$, is more than the observed oxygen surrounding the flame structure in the case of $m_p/m_s = 0.52$. Thus, another simulation was carried out with $m_p/m_s = 0.4$ by reducing the primary air.

The temperature profile along the axis of the burner at $x = 0$ m and $x = 0.05$ m is plotted from the flamelet model in Fig. 5. Along the axis of the burner (Fig. 5c), for all mass flow ratios of primary to secondary air, the temperature profile is similar. The position $y = 0$ m is marked as the origin in the burner geometry (Fig. 2b). The original burner geometry with the mass flow ratio of $m_p/m_s = 0.52$ reaches a maximum temperature of 1917 K at $y = -0.43$ m below the origin. Other mass flow ratios achieve the maximum temperature further away from the origin between $y = -0.6$ and -0.7 m. This phenomenon is observed because of the simulation strategy

Table 4 – Properties of fuel mixture.

	0% H_2	10% H_2	20% H_2	30% H_2	40% H_2	50% H_2
$\frac{\dot{m}_{(fuel)}}{\dot{m}_{(fuel-in-0\%H_2)}}$	1	0.98090	0.95871	0.93255	0.90134	0.86342
$\frac{\dot{m}_{(air)}}{\dot{m}_{(air-in-0\%H_2)}}$	1	0.99463	0.98838	0.98103	0.97225	0.96158
Lower Heating Value (MJ/m^3)	35.883	33.373	30.863	28.353	25.843	23.333

Please cite this article as: Swaminathan S et al., Numerical study of an industrial burner to optimise NO_x emissions and to evaluate the feasibility of hydrogen-enriched fuel, International Journal of Hydrogen Energy, https://doi.org/10.1016/j.ijhydene.2023.07.328

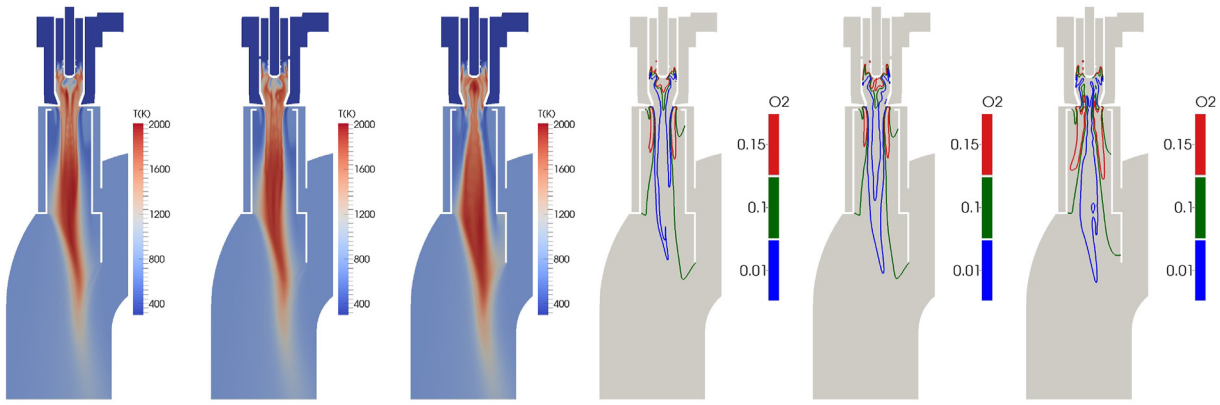

(a) m_p/m_s=0.4 (b) m_p/m_s=0.52 (c) m_p/m_s=1.4 (d) m_p/m_s=0.4 (e) m_p/m_s=0.52 (f) m_p/m_s=1.4

Fig. 4 – Temperature and mass fraction of oxygen for different mass flow ratios of primary to secondary air.

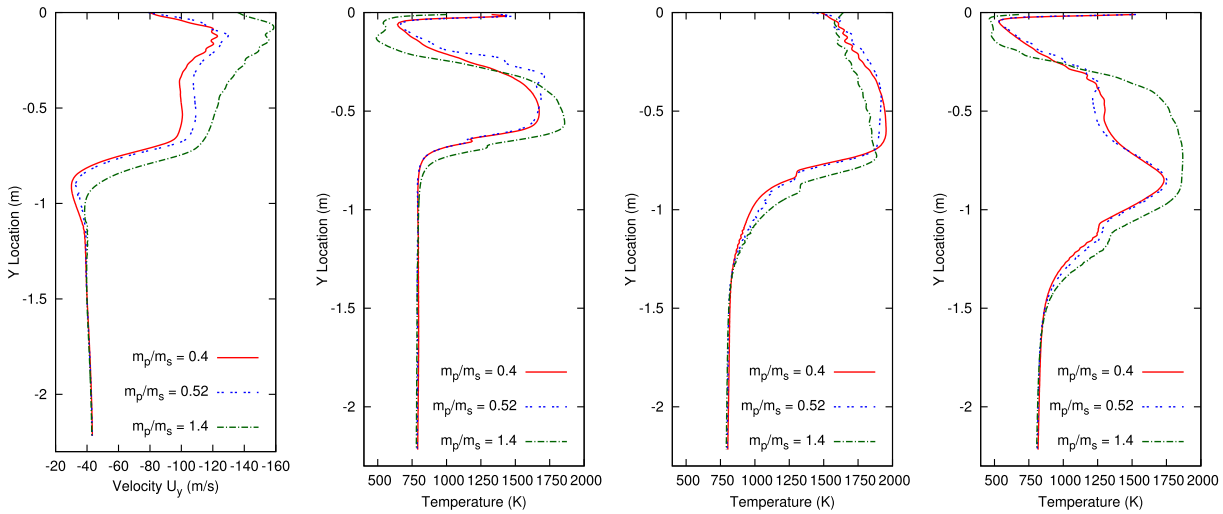

(a) At X = 0 m (b) At X = 0 m (c) At X = 0 m (d) At X = 0.05 m

Fig. 5 – Velocity and temperature profiles for different mass flow ratios of primary to secondary air.

implemented in which the ratio of 0.52 was analysed with nozzles, and other mass flow ratios were investigated with inlet patches instead of nozzles. The maximum temperatures attained along the axis of the burner were 1953 K and 1884 K by implementing mass flow ratios of 0.4 and 1.4, respectively.

Along x = 0.05 m, the maximum temperatures observed are 1731 K, 1752 K and 1868 K, and along x = −0.05 m, the maximum temperatures are 1673 K, 1711 K and 1858 K for mass flow ratios of 0.4, 0.52 and 1.4 respectively. The maximum temperature observed along x = −0.05 m and x = 0.05 m is higher for the primary to secondary air flow ratio of 1.4 as the flame width is widened, as seen in Fig. 4c, and hence higher temperatures are observed near the burner wall.

On both sides of the burner axis, near the origin (y = 0 m), the observed temperature is lower for the ratio of 1.4 as the secondary air flow nozzles are very near the measurement line. Also, the flame width is narrowed near the origin due to increased primary airflow, and the secondary air injected with ambient temperature fills in the void created by the narrowed flame. The flame developed with m_p/m_s = 1.4 does not resemble the flame observed in m_p/m_s = 0.52.

The transient simulation with a detailed chemistry solver was performed until convergence was observed by monitoring the emissions at the outlet. Fig. 6 shows the reaction rates of nitric oxide and nitrogen dioxide for m_p/m_s = 0.4, which clearly indicates the formation zones in red where excess oxygen is present in the combustion zone. The difference in NO_x emissions between different cases is not visible to the human eye as the change in reaction rates are in the order of 1×10^{-5}. Hence the normalised NO emissions are integrated at the outlet. The values are normalised with the determined NO emissions for the original mass flow ratio of m_p/m_s = 0.52. The mass flow ratio of m_p/m_s = 1.4 produces 1.382 times more NO emissions, and the ratio of 0.4 produces 0.845 times less emissions than the original burner conditions. This is mainly because of the presence of excess unburnt oxygen when increasing the primary air flow (m_p/m_s = 1.4), as in Fig. 4f, and also the higher temperatures observed near the burner wall, as in Fig. 5d. With less primary air (m_p/m_s = 0.4), the reduction rates of NO in the flame region are higher, thereby resulting in lesser NO_x emissions.

Please cite this article as: Swaminathan S et al., Numerical study of an industrial burner to optimise NO_x emissions and to evaluate the feasibility of hydrogen-enriched fuel, International Journal of Hydrogen Energy, https://doi.org/10.1016/j.ijhydene.2023.07.328

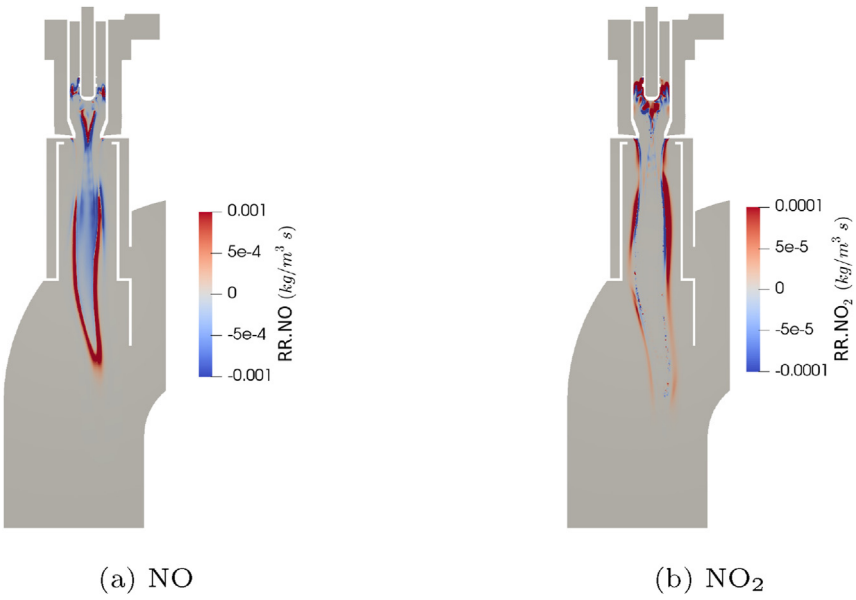

(a) NO (b) NO_2

Fig. 6 – Reaction rate of NO and NO_2 for $m_p/m_s = 0.4$.

Hence the optimum mass flow ratio of primary to secondary air to reduce NO emissions is 0.4, and a reduction in the nozzle diameter, which connects the primary and secondary airflow tubes, is required. To determine the optimum nozzle diameter, geometries with different nozzle sizes were investigated with the flamelet model by reducing the nozzle diameter step by step and the optimum mass flow ratio of primary to secondary air (m_p/m_s = 0.4) was achieved by reducing the nozzle diameter by a factor of 0.85. The change in nozzle diameter was compared with the original geometry(m_p/m_s = 0.52), and the change in temperature profile was negligible as in Fig. 5c and did not influence the combustion products.

4.2. *Investigation of the effect of hydrogen blending with natural gas*

For the investigation of hydrogen blending, the optimised burner geometry with reduced nozzle size was used. It was noticed that increasing the percentage of hydrogen in the fuel mixture results in an increase in the observed maximum temperature of the flame. Along the axis of the burner, natural gas reached a maximum temperature of 1896 K, whereas natural gas blended with 50% of hydrogen reached a maximum temperature of 1986 K. A similar behaviour of the temperature profiles was also observed by Refs. [41–44]. It could also be observed from Fig. 7a that the temperature

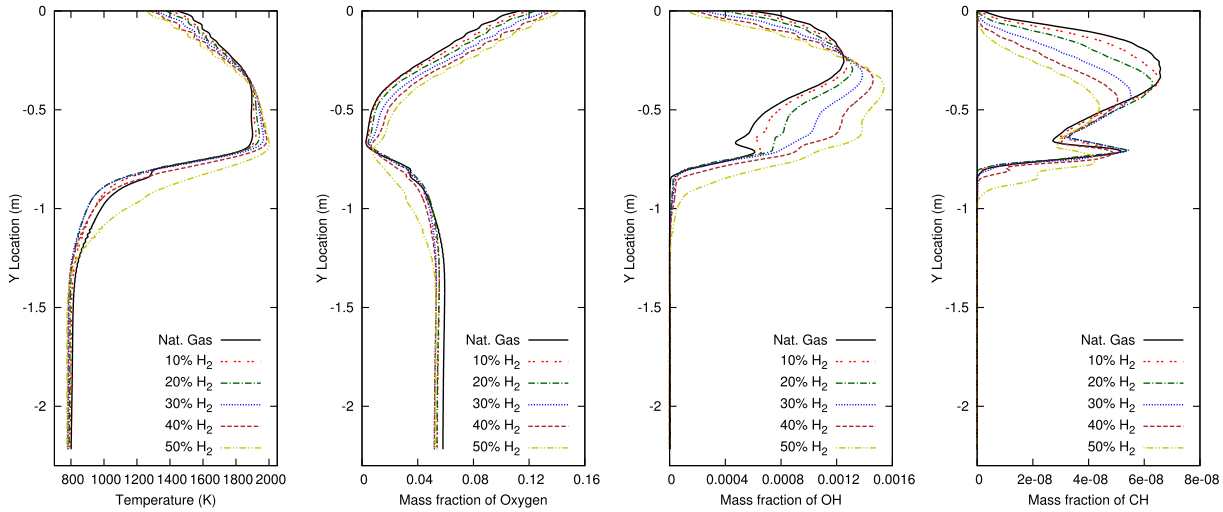

(a) (b) (c) (d)

Fig. 7 – Temperature and Mass fraction of oxygen along the axis of the burner for different gas mixtures.

Please cite this article as: Swaminathan S et al., Numerical study of an industrial burner to optimise NO_x emissions and to evaluate the feasibility of hydrogen-enriched fuel, International Journal of Hydrogen Energy, https://doi.org/10.1016/j.ijhydene.2023.07.328

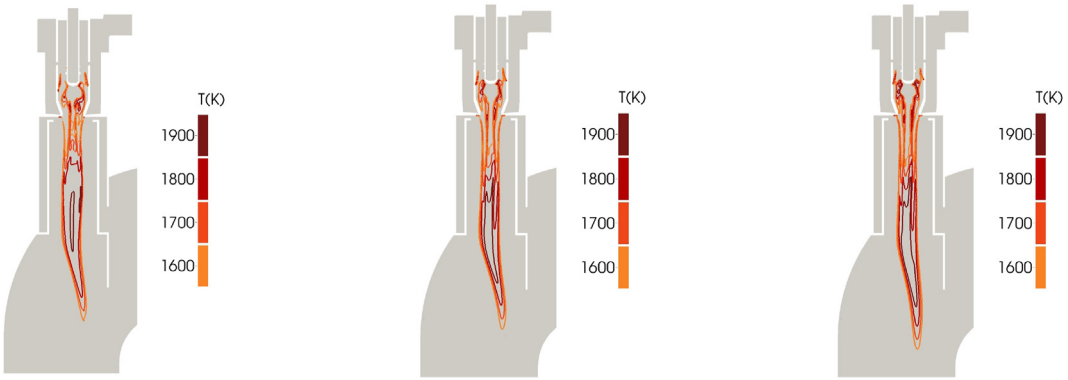

(a) Natural gas (b) 30 % of Hydrogen (c) 50 % of Hydrogen

Fig. 8 – Isocontours of temperature for different fuel compositions.

profile along the axis of the burner follows the same pattern until 40% hydrogen is added to natural gas, and when 50% of hydrogen is added, the temperature profile deviates slightly after reaching a maximum temperature. This is due to the change in flame profile, which can be observed in Fig. 8. The isocontours of 1900 K show an apparent variation in the observed profile. In the case of natural gas, the isocontours of 1900 K are smaller, and as the percentage of hydrogen increases, the contour profile is elongated. Moreover, a minimal increase in the flame length could be observed by comparing the isocontours of 1600 K. Ge et al. [45] conducted experiments with a radially-staged dry low emission burner for various volume content of hydrogen and observed that the flame shrinks as the hydrogen content increases when the volumetric flow remains constant. The same flame behaviour is also observed by Leicher et al. [46], and also the NO_x emissions increase tremendously when the volume flows of both fuel and oxidizer remain unchanged. They also observed that the measured NO_x emissions remain almost the same when both the firing rate and the air excess ratio are kept constant. In this study, the volumetric flow of both fuel and air was altered to maintain a stable burner power output and, consequently, did not influence the length of the flame to a greater extent. From Fig. 7c and d, it could be observed that increasing the hydrogen content in the fuel mixture reduces the amount of CH and increases the amount of OH. The oxygen mass fractions (Fig. 7b) reduce with higher hydrogen content until y = −0.6 m, and further down, increases due to the presence of oxygen in the circulated furnace atmosphere.

Fig. 9a shows the carbon monoxide and carbon dioxide emissions at the outlet obtained from the flamelet model. Increasing the percentage of hydrogen results in a steady decrease in CO and CO_2 emissions for more than 10% of hydrogen in the fuel mixture. In the case of blending natural gas with 10% of hydrogen, CO increased by 8.95%, and CO_2 increased by 0.8%. Maximum reduction was observed with 50% of hydrogen in the fuel mixture, decreasing 76.8% of CO and 15.76% of CO_2 emissions as also observed by Refs. [11,47–49]. A significant parameter to be considered in interpreting these emission results is that the mass flow of the circulated furnace atmosphere is held constant for all fuel mixtures. As mentioned in Table 4, the mass flow of both air and fuel decreases steadily when increasing the amount of hydrogen in the mixture. This can cause an increase in CO and CO_2 emissions in the case of the fuel mixture with 10% of hydrogen as the circulated furnace atmosphere also contains

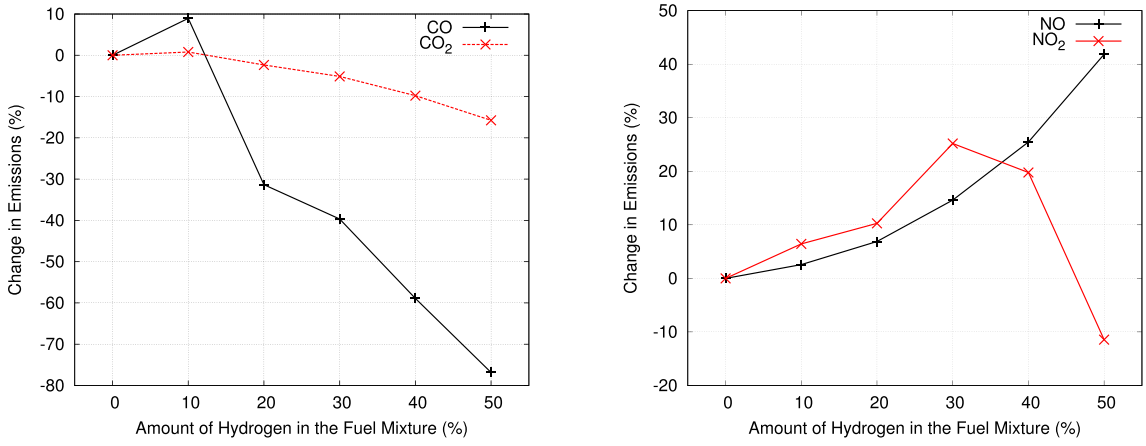

(a) CO and CO_2 emissions from flamelet model (b) NO and NO_2 emissions from NO_x model

Fig. 9 – Change in carbon and nitrogen emissions measured at the outlet.

Please cite this article as: Swaminathan S et al., Numerical study of an industrial burner to optimise NO_x emissions and to evaluate the feasibility of hydrogen-enriched fuel, International Journal of Hydrogen Energy, https://doi.org/10.1016/j.ijhydene.2023.07.328

a limited amount of CO. This increase could not be observed in other gas mixtures as the reduction in CO and CO_2 emissions is larger than the limited CO present in the circulated furnace atmosphere.

NO_x emissions at the outlet were obtained from the NO_x model, as in Fig. 9b. Nitrogen oxide emissions increase rapidly as the percentage of hydrogen in the fuel mixture increases. With 50% hydrogen in the fuel mixture, an increase of 41.8% NO was detected. On the contrary, NO_2 increased until 40% of hydrogen was blended in the fuel mixture, and in the case of 50% of hydrogen in the fuel mixture, a decrease of 11.4% in NO_2 emissions were detected. This behaviour can be attributed to the difference in temperature and oxygen profiles of the flame with 50% of hydrogen as in Fig. 7, and also an abrupt increase of 24.8% of N_2O emissions was observed with 50% of hydrogen compared with the N_2O emissions from 40% of hydrogen in the fuel mixture. Similar behaviour with an increase in NO emissions was also observed by Wu et al. [50] and Rortveit and Hustad [51]. This increase in NO emissions was still under the permissible limits according to EG-L [3] regulations. Hence, it is evident from the numerical investigations that the modelled burner exhibits similar flame characteristics until 40% of the hydrogen is added to natural gas.

5. Conclusion

The developed numerical model successfully predicted NO_x emissions in alignment with experimental studies. To mitigate NO_x emissions from an industrial burner, modifications were made to the mass flow of primary and secondary air. By adopting a primary to secondary air mass flow ratio of 0.4, NO emissions decreased by a factor of 0.845. To achieve the optimal mass flow ratio, the nozzle diameter needed to be reduced by a factor of 0.85.

Furthermore, the enhanced burner design was evaluated for its impact on enriching natural gas with up to 50% hydrogen by volume, while maintaining a constant power output. The burner exhibited similar flame characteristics until 40% hydrogen was added to the natural gas. However, the addition of 50% hydrogen resulted in a 76.8% reduction in CO emissions, a 15.76% reduction in CO_2 emissions, and a 41.8% increase in NO emissions. Further enhancements to the numerical investigation could involve varying the amount of circulated furnace atmosphere rather than relying on a constant value.

Declaration of competing interest

The authors declare that they have no known competing financial interests or personal relationships that could have appeared to influence the work reported in this paper.

Acknowledgement

The authors gratefully acknowledge the funding support of K1-MET GmbH, metallurgical competence center. The research program of the K1-MET competence center is supported by COMET (Competence Center for Excellent Technologies), the Austrian program for competence centers. COMET is funded by the Federal Ministry for Climate Action, Environment, Energy, Mobility, Innovation and Technology, the Federal Ministry for Digital and Economic Affairs, the Federal States of Upper Austria, Tyrol and Styria, as well as the Styrian Business Promotion Agency (SFG) and the Standortagentur Tyrol. Furthermore, we thank Upper Austrian Research GmbH for its continuous support. The authors gratefully acknowledge the funding support from the Industrial Partner Ebner Industrieofenbau GmbH. The authors also thank Emerson Edilson Barros de Souza and Yangyue Pan for their support.

REFERENCES

[1] Chossière GP, Malina R, Ashok A, Dedoussi IC, Eastham SD, Speth RL, Barrett SR. Public health impacts of excess nox emissions from volkswagen diesel passenger vehicles in Germany. Environ Res Lett 2017;12:34014.
[2] EEA. Air quality in Europe - report. Technical Report. European Environmental Agency; 2022. https://doi.org/10.2800/488115. URL: https://www.eea.europa.eu/publications/air-quality-in-europe-2022/sources-and-emissions-of-air.
[3] EG-L. Bundesgesetz über nationale emissionsreduktionsverpflichtungen für bestimmte luftschadstoffe (emissionsgesetz-luft 2018 – eg-l 2018), Bundesgesetzblatt für die Republik Österreich. 2018.
[4] Skalska K, Miller JS, Ledakowicz S. Trends in nox abatement: a review. Sci Total Environ 2010;408:3976–89.
[5] Lopez-Ruiz G, Fernandez-Akarregi A, Diaz L, Urresti I, Alava I, Blanco J. Numerical study of a laminar hydrogen diffusion flame based on the non-premixed finite-rate chemistry model; thermal nox assessment. Int J Hydrogen Energy 2019;44:20426–39.
[6] Pitsch H. Improved pollutant predictions in large-eddy simulations of turbulent non-premixed combustion by considering scalar dissipation rate fluctuations. Proc Combust Inst 2002;29:1971–8.
[7] Vreman A, Albrecht B, van Oijen J, de Goey L, Bastiaans R. Premixed and nonpremixed generated manifolds in large-eddy simulation of sandia flame d and f. Combust Flame 2008;153:394–416.
[8] Vujanovicć M, Duić N, Tatschl R. Validation of reduced mechanisms for nitrogen chemistry in numerical simulation of a turbulent non-premixed flame. React Kinet Catal Lett 2009;96:125–38.
[9] Pollhammer W, Spijker C, Raupenstrauch H, Koller M. Development of a two step simulation concept for fast and accurate prediction of nox using flamelet model and detailed chemistry in openfoam. In: Proceedings of 14th minisymposium verfahrenstechnik (JKU linz); 2018. URL: http://www.chemical-engineering.at/conference/index.php/proc_miniVT/proc2018.
[10] Swaminathan S, Spijker C, Raupenstrauch H, Kofler I, Koller M. New developments to the post-processor in determining nitrogen oxide emissions with an computationally efficient approach. Carbon Resources Conversion 2020;3:198–202.
[11] Cellek MS, Pınarbaşı A. Investigations on performance and emission characteristics of an industrial low swirl burner while burning natural gas, methane, hydrogen-enriched natural gas and hydrogen as fuels. Int J Hydrogen Energy 2018;43:1194–207.

Please cite this article as: Swaminathan S et al., Numerical study of an industrial burner to optimise NO_x emissions and to evaluate the feasibility of hydrogen-enriched fuel, International Journal of Hydrogen Energy, https://doi.org/10.1016/j.ijhydene.2023.07.328

[12] Mayrhofer M, Koller M, Seemann P, Prieler R, Hochenauer C. Assessment of natural gas/hydrogen blends as an alternative fuel for industrial heat treatment furnaces. Int J Hydrogen Energy 2021;46:21672–86.
[13] Zhang G-P, Li G-X, Li H-M, Lv J-C. Experimental study on the effect of diluent gas on h2/co/air mixture turbulent premixed flame. Int J Hydrogen Energy 2022;47:610–23.
[14] Van Der Drift A, Tjeng S, Beckers G, Beesteheerde J. Low-nox hydrogen burner. Int J Hydrogen Energy 1996;21:445–9.
[15] Choudhuri AR, Gollahalli S. Characteristics of hydrogen–hydrocarbon composite fuel turbulent jet flames. Int J Hydrogen Energy 2003;28:445–54.
[16] Cozzi F, Coghe A. Behavior of hydrogen-enriched non-premixed swirled natural gas flames. Int J Hydrogen Energy 2006;31:669–77.
[17] Cuoci A, Frassoldati A, Faravelli T, Ranzi E. Kinetic modeling of soot formation in turbulent nonpremixed flames. Environ Eng Sci 2008;25:1407–22.
[18] Cuoci A, Frassoldati A, Faravelli T, Ranzi E. Formation of soot and nitrogen oxides in unsteady counterflow diffusion flames. Combust Flame 2009;156:2010–22.
[19] Greenshields CJ, et al. Openfoam user guide. OpenFOAM Foundation Ltd; 2015. p. 47. version 3.
[20] Launder BE, Spalding DB, et al. Lectures in mathematical models of turbulence. 1972.
[21] Raithby G, Chui E. A finite-volume method for predicting a radiant heat transfer in enclosures with participating media. 1990.
[22] Smith T, Shen Z, Friedman J. Evaluation of coefficients for the weighted sum of gray gases model. 1982.
[23] Peters N. Laminar diffusion flamelet models in non-premixed turbulent combustion. Prog Energy Combust Sci 1984;10:319–39.
[24] Ihme M, Pitsch H. Modeling of radiation and nitric oxide formation in turbulent nonpremixed flames using a flamelet/progress variable formulation. Phys Fluids 2008;20:55110.
[25] Cutrone L, De Palma P, Pascazio G, Napolitano M. A rans flamelet–progress-variable method for computing reacting flows of real-gas mixtures. Comput Fluids 2010;39:485–98.
[26] Smith GP, Golden DM, Frenklach M, Moriarty NW, Eiteneer B, Goldenberg M, Bowman CT, Hanson RK, Song S, Gardiner Jr WC, Lissianski V, Qin Z. Gri 3.0 mechanism. Gas Research Institute; 1999.
[27] Barlow R, Frank J. Piloted ch4/air flames c, d, e, and f–release 2.1 15-jun-2007. 2007. URL: https://tnfworkshop.org/wp-content/uploads/2019/02/SandiaPilotDoc21.pdf.
[28] Zahirović S, Scharler R, Kilpinen P, Obernberger I. Validation of flow simulation and gas combustion sub-models for the cfd-based prediction of nox formation in biomass grate furnaces. Combust Theor Model 2010;15:61–87.
[29] Sheikhi M, Drozda T, Givi P, Jaberi F, Pope S. Large eddy simulation of a turbulent nonpremixed piloted methane jet flame (sandia flame d). Proc Combust Inst 2005;30:549–56.
[30] Yue C, Wang J, Li X. Modeling of sandia flame d with the non-adiabatic chemistry tabulation approach: the effects of different laminar flames on no x prediction. RSC Adv 2023;13:4590–600.
[31] Lysenko DA, Ertesvåg IS, Rian KE. Numerical simulations of the sandia flame d using the eddy dissipation concept. Flow, Turbul Combust 2014;93:665–87.
[32] Barlow R, Frank J. Effects of turbulence on species mass fractions in methane/air jet flames. In: Symposium (international) on combustion, vol. 27. Elsevier; 1998. p. 1087–95.
[33] Zeldvich YB. The oxidation of nitrogen in combustion and explosions. J. Acta Physicochimica 1946;21:577.
[34] Heywood JB. Internal combustion engine fundamentals. McGraw-Hill, Inc.; 1988.
[35] Spijker C, Swaminathan S, Raupenstrauch H. A numerically efficient method for the prediction of nitrogen oxide emissions in industrial furnaces. Steel Res Int 2020;91:2000239.
[36] A. F. U. Guide, release 14.0. USA: ansys, Inc.; 2011. November.
[37] Fluent A, et al. Ansys fluent theory guide, vol. 15317. USA: Ansys Inc.; 2011. p. 724–46.
[38] Skreiberg Ø, Hustad J, Karlsvik E. Empirical no x-modelling and experimental results from wood stove combustion: empirical no x-modelling and experimental results. Developments in Thermochemical Biomass Conversion: Volume 1/Volume 2 1997:1462–76.
[39] Houshfar E, Skreiberg O, Lovas T, Todorovic D, Sorum L. Effect of excess air ratio and temperature on nox emission from grate combustion of biomass in the staged air combustion scenario. Energy Fuels 2011;25:4643–54.
[40] Spliethoff H, Greul U, Rüdiger H, Hein KR. Basic effects on nox emissions in air staging and reburning at a bench-scale test facility. Fuel 1996;75:560–4.
[41] Ziani L, Chaker A, Chetehouna K, Malek A, Mahmah B. Numerical simulations of non-premixed turbulent combustion of ch4–h2 mixtures using the pdf approach. Int J Hydrogen Energy 2013;38:8597–603.
[42] Oh J, Noh D, Ko C. The effect of hydrogen addition on the flame behavior of a non-premixed oxy-methane jet in a lab-scale furnace. Energy 2013;62:362–9.
[43] Gao X, Duan F, Lim SC, Yip MS. Nox formation in hydrogen–methane turbulent diffusion flame under the moderate or intense low-oxygen dilution conditions. Energy 2013;59:559–69.
[44] Francis KA, Sreenivasan R, Raghavan V. Investigation of structures and reaction zones of methane–hydrogen laminar jet diffusion flames. Int J Hydrogen Energy 2011;36:11183–94.
[45] Ge B, Ji Y, Zhang Z, Zang S, Tian Y, Yu H, Chen M, Jiao G, Zhang D. Experiment study on the combustion performance of hydrogen-enriched natural gas in a dle burner. Int J Hydrogen Energy 2019;44:14023–31.
[46] Leicher J, Nowakowski T, Giese A, Görner K. Hydrogen in natural gas: how does it impact industrial end users. In: Proceedings of the world gas conference; 2018.
[47] Büyükakın MK, Öztuna S. Numerical investigation on hydrogen-enriched methane combustion in a domestic back-pressure boiler and non-premixed burner system from flame structure and pollutants aspect. Int J Hydrogen Energy 2020;45:35246–56.
[48] Okosun T, Nielson S, Zhou C. Blast furnace hydrogen injection: investigating impacts and feasibility with computational fluid dynamics. J Occup Med 2022;74:1521–32.
[49] Guo H, Smallwood GJ, Liu F, Ju Y, Gülder ÖL. The effect of hydrogen addition on flammability limit and nox emission in ultra-lean counterflow ch4/air premixed flames. Proc Combust Inst 2005;30:303–11.
[50] Wu L, Kobayashi N, Li Z, Huang H, Li J. Emission and heat transfer characteristics of methane–hydrogen hybrid fuel laminar diffusion flame. Int J Hydrogen Energy 2015;40:9579–89.
[51] Rortveit G, Hustad J. No x formations in diluted ch 4/h 2 counterflow diffusion flames. Int J Energy a Clean Environ (IJECE) 2003;4.

Please cite this article as: Swaminathan S et al., Numerical study of an industrial burner to optimise NO_x emissions and to evaluate the feasibility of hydrogen-enriched fuel, International Journal of Hydrogen Energy, https://doi.org/10.1016/j.ijhydene.2023.07.328